Available online at www.sciencedirect.com
ScienceDirect
Journal of Catalysis 250 (2007) 171–183
JOURNAL OF CATALYSIS
www.elsevier.com/locate/jcat

Proton exchange of small hydrocarbons over acidic chabazite: Ab initio study of entropic effects

Tomáš Bučko [a,*], Lubomir Benco [a], Jürgen Hafner [a], János G. Ángyán [b]

[a] *Fakultät für Physik and Center for Computational Materials Science, Universität Wien, Sensengasse, 1090 Wien, Austria*
[b] *Laboratoire de Cristallographie et Modélisation des Matériaux Minéraux et Biologiques, UMR 7565, CNRS – Nancy-Université, B.P. 239, F-54506 Vandœuvre-lès-Nancy, France*

Received 4 April 2007; revised 23 May 2007; accepted 30 May 2007

Available online 12 July 2007

Abstract

The proton-exchange reaction of a series of short hydrocarbons over an acidic zeolite (chabazite) was studied using periodic density functional theory (DFT) calculations. It was found that the chain length of hydrocarbons does not have a significant effect on the height of the potential-energy barrier. The experimentally observed regioselectivity between methyl and methylene groups in propane and between methyl and methine groups in isobutane was shown to be an entropic effect. In addition to the direct H-exchange, a mechanism mediated by a methylpropene molecule recently suggested by experimentalists was explored. It was found that entropy plays a very important role in driving the reaction.

Keywords: Ab initio; Molecular dynamics; Free-energy; Entropy; Proton exchange; Zeolites

1. Introduction

Acidic zeolites are frequently used as catalysts in hydrocarbon transformations, such as cracking, isomerization, and alkylation. Despite decades of experimental investigation and heavy industrial use, the detailed mechanism for the activation of the C–C and C–H bonds of rather inert alkanes remains unclear. A simple prototypical reaction to study C–H bond activation is the proton exchange between short hydrocarbons and an acidic zeolite. In what follows, we summarize some important experimental facts concerning this reaction. Experimentally determined apparent activation energies for different short alkanes are collected in Table 1.

The simplest reaction—proton exchange between methane and the bridging OH groups in the zeolites ZSM-5 and FAU—was studied by means of IR spectroscopy and ab initio calculations by Kramer et al. [1]. At a sufficiently low partial pressure of methane, the only realistic mechanism is a direct H-exchange (Scheme 1) in which a penta-coordinated alkanium cation (2) is created as a transition state. The apparent activation energy reported by Kramer et al. [1] is ∼130 kJ/mol. Similar values were found for reactions catalyzed by two different zeolites, ZSM-5 and FAU. More recently, Engelhardt et al. [2,3] measured H/D exchange between deuterated methane CD_4 and the OH groups of various H-zeolites and γ-Al_2O_3, which showed no Brønsted acidity even against strong Brønsted bases. It was demonstrated that Lewis sites present in zeolites actively participate in the reaction, lowering the macroscopic activation energy significantly. The measured apparent activation energies varied between 26 and 86 kJ/mol, significantly lower than the

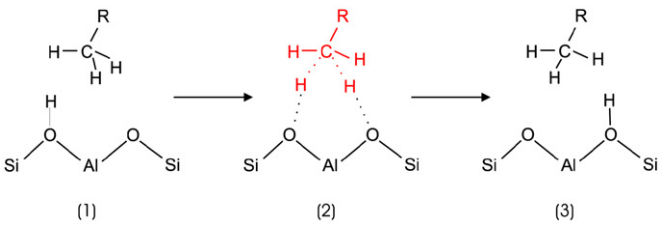

Scheme 1.

* Corresponding author.
E-mail address: tomas.bucko@univie.ac.at (T. Bučko).

0021-9517/$ – see front matter
doi:10.1016/j.jcat.2007.05.025

Table 1
Experimental apparent activation energies ($\Delta E^{\ddagger,\mathrm{app}}$) for the proton exchange reaction and heats of adsorption (ΔH_{ads}) for short alkanes over acidic zeolites. Heat of adsorption for methane is extrapolated from data in Ref. [30]

Alkane	$\Delta E^{\ddagger,\mathrm{app}}$ (kJ/mol)	Zeolite	Ref.	ΔH_{ads} (Ref. [30]) (kJ/mol)	$\Delta E^{\ddagger,\mathrm{app}} - \Delta H_{\mathrm{ads}}$ (kJ/mol)
Methane	130	H-FAU, H-ZSM-5	[39]	−22	152
Ethane	–				
Propane				−46	
(prim. C)	108 ± 7	H-ZSM-5	[4]		154
	107 ± 10	H-ZSM-5	[6]		153
(sec. C)	117 ± 7	H-ZSM-5	[4]		163
	125 ± 6	H-ZSM-5	[6]		171
n-Butane	85	H-ZSM-5	[7]	−58	143
Isobutane					
(prim. C)	50 ± 2	H-ZSM-5	[8]	−52	102
	57	H-ZSM-5	[9]		109
(tert. C)	–				

values reported by Kramer et al. [1]. Clearly, not only the Brønsted acidity, but also the zeolite topology and the Lewis acidity, are important parameters for this reaction. In this work, we focus attention on H-exchange reactions that take place through the intermediary of a Brønsted site.

Whereas for methane, the most likely mechanism is a direct H-exchange, for longer alkanes, other alternatives also should be considered. The mechanism of H/D exchange of deuterated propane with the zeolite H-ZSM-5 was studied by Stepanov et al. [4–6]. The direct mechanism was found to be dominant over a bimolecular reaction in which an unsaturated hydrocarbon plays the role of a co-catalyst. Furthermore, regioselectivity between methyl and methylene groups of propane was observed [4,5]. The methyl groups were shown to exchange a proton about three times faster than the methylene group. Remarkably, the measured activation energies for reactions involving the methyl and methylene groups were the same within the experimental error (see Table 1).

Lercher et al. [7] measured an apparent activation energy of 85 kJ/mol for the proton exchange between *n*-butane and H-ZSM-5. A direct mechanism was assumed a priori, and the regioselectivity between the CH_3 and CH_2 groups was not discussed in detail. The mechanism of the H/D exchange between isobutane and acid zeolites continues to be a controversial subject. On one hand, Sommer et al. [8] suggested that the reaction proceeds via a bimolecular mechanism involving a methylpropene molecule. The individual steps of this mechanism are described in detail in Section 5. On the other hand, Truitt et al. [9] came to a quite different conclusion that, in close analogy to other short alkanes, the reaction proceeds via a direct mechanism. Remarkably, both authors agree in two other important aspects: (i) the reaction is regioselective; that is, only the methyl groups exchange protons with the zeolite, and (ii) the apparent activation energy is ∼50 kJ/mol, significantly lower compared with other short alkanes.

In this paper we address three experimentally relevant questions: (i) How does the activation energy for proton exchange depend on the geometry of short alkanes? (ii) What is the reason for the experimentally observed regioselectivity between the methyl and methylene groups of propane, and between the CH_3 and CH groups of isobutane? (iii) Which mechanism, direct or mediated, is preferable for proton exchange between isobutane and a zeolite? The paper is organized as follows: In Section 2, we introduce the methodology and describe details of the simulations used in this study. In Section 3, we determine stationary points and corresponding potential energies for the direct proton exchange of a series of short alkanes. In Section 4, we analyze entropic effects on the direct mechanism. We discuss the mediated (bimolecular) mechanism for proton exchange of isobutane in Section 5, and summarize the most important results of this work in Section 6.

2. Computational details

2.1. Structural model

Acidic chabazite with one Al site per a simulation cell, corresponding to a Si/Al ratio of Si/Al = 23, was used as a model zeolite system. In all initial configurations, the acid proton was located in position O4 according to the nomenclature used by Jeanvoine et al. [10]. Lattice parameters were derived from the experimental geometry determined for a highly siliceous form (SSZ-13) of chabazite [11] ($R\bar{3}m$, $a = 9.291$ Å, $\alpha = 93.92°$). To avoid undesired interactions between the images of the reactive domain containing the acid site and the hydrocarbon molecule, a larger simulation cell was used (see Fig. 1). The lattice vectors of the larger cell (**a**, **b**, **c**) are related to those of

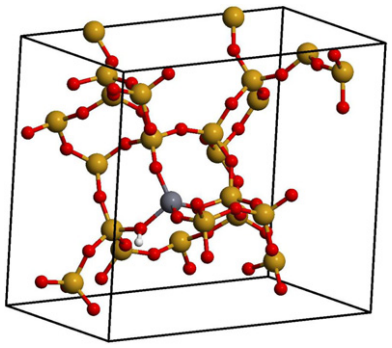

Fig. 1. Simulation cell for acidic chabazite used in this study.

the original cell ($\mathbf{a_1}$, $\mathbf{a_2}$, $\mathbf{a_3}$) via transformations $\mathbf{a} = \mathbf{a_1} + \mathbf{a_2}$, $\mathbf{b} = \mathbf{a_1} - \mathbf{a_2}$, and $\mathbf{c} = \mathbf{a_3}$, leading to a cell with lattice parameters $a = 12.682$ Å, $b = 13.581$ Å, $c = 9.291$ Å, $\alpha = 90.00°$, $\beta = 95.74°$, and $\gamma = 90.00°$. This periodically repeated cell contains 24 tetrahedral TO_2 units: one AlO_4 and 23 SiO_4 tetrahedra.

2.2. Electronic structure calculation

Periodic ab initio DFT calculations were performed using the VASP code [12–15]. The Kohn–Sham equations were solved variationally in a plane-wave basis set using the projector-augmented wave (PAW) method of Blöchl [18], as adapted by Kresse and Joubert [19]. The exchange-correlation energy was described by the PW91 generalized gradient approximation (GGA) functional [16,17]. Brillouin zone sampling was restricted to the Γ-point. During geometry optimizations, the plane-wave cutoff was set to 400 eV, whereas in the molecular dynamics simulations a smaller cutoff (300 eV) was used to save computer time. In the optimization runs, the convergence criterion for the electronic self-consistency cycle, measured by the change in the total energy between successive iterations, was set to 10^{-5} eV/cell, whereas it was 10^{-4} eV/cell in the case of the MD simulations.

2.3. Geometry optimizations

Relaxation of the atomic positions was carried out using a conjugate-gradient algorithm minimization of energies and forces. Transition structures were identified using the dimmer method [20], as recently improved by Heyden et al. [21]. Atomic positions were considered to be relaxed if all forces acting on the atoms were <0.03 eV/Å.

2.4. Molecular dynamics and the free-energy calculations

Molecular dynamics simulations were performed in the NVT ensemble. The temperature of 300 K was controlled using a Nosé–Hoover thermostat [22,23]. An integration step of 1 fs was used. The atomic mass of tritium was used for all H atoms, to avoid thermal separation of "hard" modes, such as the O–H and C–H stretching modes, from softer lattice modes. The free-energy profiles for the reactions were calculated using the Blue Moon ensemble method [24] for sampling rare events, in a variant adapted for vectorial constraints [25–27] as described in Appendix A.

3. Direct reaction mechanism

3.1. Potential energy for stationary points

Direct proton exchange between an alkane and a Brønsted acid site is a simple one-step reaction. Once the alkane has approached the Brønsted acid site, an adsorption complex is created. As an example, the structure of the adsorption complex of ethane is shown in Fig. 2a. Similar adsorption complexes are formed by other short alkanes, as illustrated by a list of some of their important internal parameters, compiled in Table 2. Because these potential-energy minima were obtained by relaxing slightly perturbed transition structures, we cannot *a priori* exclude the existence of even more stable configurations, corresponding to a variation of the soft degrees of freedom, such as hindered rotations and translations.

Calculated interaction energies between alkanes and acidic chabazite are all about 10 kJ/mol (see Table 3), practically

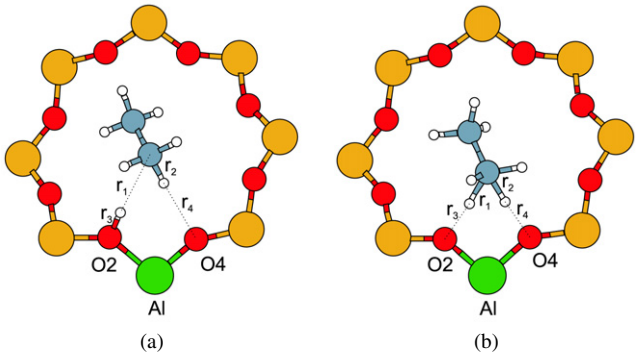

Fig. 2. Detailed view of the adsorption complex of ethane at a Brønsted acid site in chabazite (a) and transition state for proton-exchange (b). Corresponding values for the interatomic distances $r_1 - r_4$ for methane, ethane, propane, *n*-butane, and isobutane are compiled in Table 2.

Table 2
Selected interatomic distances (Å) for adsorption complexes and transition state configurations for direct proton exchange between short hydrocarbons and Brønsted acid sites in chabazite. For the adsorption complex, r_1 and r_4 describe the length of the C–H_{Zeo} and O_{Zeo}–H hydrogen bonds, respectively. For the transition state r_3 and r_4 measure the lengths of the hydrogen bonds between the protonated alkane and oxygen atoms of the zeolite, r_2 measures the length of the C–H bond in the hydrocarbon forming a weak hydrogen bond to a framework oxygen (cf. Fig. 2). The values in parentheses correspond to results optimized with the lower plane-wave cutoff as used in MD calculations (see Section 2.2 for details)

	Adsorption complex				Transition state			
	r_1	r_2	r_3	r_4	r_1	r_2	r_3	r_4
Methane	2.47	1.10	0.98	3.64	1.27	1.29	1.45	1.45
Ethane	2.35	1.11	0.99	2.52	1.26	1.28	1.49	1.49
Propane (prim. C)	2.40	1.11	0.99	2.52	1.26	1.28	1.50	1.50
Propane (sec. C)	2.51	1.11	0.98	2.55	1.27	1.27	1.52	1.55
n-Butane (prim. C)	2.47	1.10	0.98	2.43	1.26	1.27	1.49	1.51
n-Butane (sec. C)	2.68	1.11	0.98	2.64	1.27	1.27	1.54	1.58
Isobutane (prim. C)	2.53 (2.55)	1.10 (1.11)	0.98 (0.98)	2.72 (2.72)	1.23 (1.26)	1.30 (1.31)	1.54 (1.48)	1.51 (1.47)
Isobutane (tert. C)	2.50 (2.51)	1.11 (1.12)	0.98 (0.98)	2.69 (2.70)	1.24 (1.26)	1.37 (1.38)	1.64 (1.60)	1.53 (1.50)

Table 3
Calculated adsorption energies (ΔE_{ads}) and true activation energies ($\Delta E^{\ddagger}$) for the proton-exchange reaction. The values in parentheses correspond to results optimized with the same reduced plane wave cutoff as used in MD calculations (see Section 2.2 for details)

	ΔE_{ads} (kJ/mol)	$\Delta E^{\ddagger}$ (kJ/mol)
Methane	−11	117
Ethane	−10	113
Propane (prim. C)	−15	115
Propane (sec. C)	−11	110
n-Butane (prim. C)	−9	117
n-Butane (sec. C)	−16	119
Isobutane (prim. C)	−9 (−11)	127 (112)
Isobutane (tert. C)	−14 (−13)	139 (125)

independent of the hydrocarbon chain length, but experimental interaction energies increase linearly with the hydrocarbon length in increments of 8–14 kJ/mol, depending on the pore size and tortuosity of the zeolite [28–30] (see Table 1). The discrepancy between the experimental and theoretical results is due to the well-known failure of standard DFT techniques to describe van der Waals interactions [31]. In fact, the values reported here are close to the specific interaction energy between hydrocarbons and a Brønsted acid site of ∼10 kJ/mol, determined experimentally by Eder and Lercher [28]. A detailed ab initio DFT study of the adsorption of linear hydrocarbons in zeolites can be found in Ref. [32].

After the formation of an adsorption complex, the proton transfer can occur. The transition structure (see Fig. 2b) is a penta-coordinated alkanium cation, where two hydrogen atoms interact with two framework oxygen atoms. The transition state geometries for linear hydrocarbons are all rather similar. Some important internal parameters for different transition structures are compiled in Table 2. The reaction is completed when one of the interacting hydrogen atoms jumps to a framework oxygen atom and forms a Brønsted acid site. The calculated activation energies for a series of hydrocarbons are compiled in Table 3. For linear hydrocarbons, the activation energies show no obvious trend with respect to the length of the molecule, with all values lying between 110 and 119 kJ/mol. The potential-energy barriers for reactions involving two different functional groups in the isobutane are higher compared with linear hydrocarbons, $\Delta E^{\ddagger} = 127$ kJ/mol for methyl and $\Delta E^{\ddagger} = 139$ kJ/mol for methine groups.

Our results can be compared with the vast amount of theoretical and experimental data available. The activation energies from available quantum-chemical studies are compiled in Table 4. Note that in these investigations, the zeolite was represented by a small cluster involving only three to five tetrahedral sites (i.e., Si or Al atoms). Therefore, the interaction of the hydrocarbon with the zeolite framework beyond the active site was completely neglected.

Esteves et al. [33] studied the proton-exchange reaction for methane, ethane, propane, and isobutane at the B3LYP and MP2 levels of theory. The activation energies calculated using the B3LYP functional were almost constant along the series of linear hydrocarbons ($\Delta E^{\ddagger} = \sim 135$ kJ/mol). The barrier for a reaction involving a methylene group of propane was only slightly higher ($\Delta E^{\ddagger} = \sim 139$ kJ/mol) than that involving primary carbon atoms. More significant is the difference in $\Delta E^{\ddagger}$ between the CH_3 and CH groups of isobutane, the latter being higher by ∼17 kJ/mol.

The activation energies obtained via the MP2 method decreased from 130 kJ/mol for methane to 125 kJ/mol for the methyl group of isobutane. Whereas there was no appreciable difference in $\Delta E^{\ddagger}$ between the CH_3 and CH_2 groups of propane (both are ∼128 kJ/mol), the calculated activation energy for the methine group of isobutane was ∼7 kJ/mol greater than that for a methyl group. Ryder et al. [34] used BH&HLYP hybrid functionals to calculate activation energies for reactions involving methane, ethane, and propane. Again, the calculated activation energies for all alkanes were very similar, with the largest difference being 6 kJ/mol. In a series of papers, Zheng et al. [35–38] published studies on proton exchange for the same series of short alkanes as considered in this study. Structures were optimized using the B3LYP method, and energies were calculated using the CBS-QB3 composite energy method, providing complete basis set (CBS) total energy estimates. The calculated activation energies decreased slightly with increasing hydrocarbon length. However, except for methane, the differences were very small. Moreover, the differences between different functional groups in propane and in isobutane were only a few kJ/mol. Altogether, all theoretical simulations failed to predict

Table 4
The ZPE-corrected true activation energies ($\Delta E^{\ddagger}$) calculated for proton-exchange between alkanes and acidic zeolite at different levels of theory

		$\Delta E^{\ddagger}$ (kJ/mol)			
Reference		Esteves et al. [33]		Ryder et al. [34]	Zheng and Blowers [35–38]
Level of theory		B3LYP/6-31G*	MP2/6-31G*	BH&HLYP/6-31++G**	B3LYP/6-31G*, CBS-QB3
Alkane	Active group				
Methane	CH_4	135	130	167	140
Ethane	CH_3	135	131	170	130
Propane	CH_3	135	128	170	127
Propane	CH_2	139	128	164	125
n-Butane	CH_3	–	–	–	125
n-Butane	CH_2	–	–	–	119
Isobutane	CH_3	135	125	–	123
Isobutane	CH	152	132	–	125

significant trends in the activation energies in the series of short alkanes.

Thus, at first sight, the theoretical results seem to be in disagreement with the experimental results. As shown in Table 1, the measured activation energies decreased from 130 kJ/mol for methane over ∼110 kJ/mol for propane to 85 kJ/mol for butane. However, these "apparent" activation energies should be corrected by subtracting the negative heat of adsorption to obtain the higher "true" activation energies comparable with calculations [39], which describe the energy change between the adsorption complex and the transition structure. In fact, after having performed this correction, we find that, as predicted by theory, the activation energies are almost independent of chain length. Obviously, our theoretically predicted barriers are ∼30–40 kJ/mol too low compared with corrected experimental activation energies. However, as we show later, theoretical activation energies increased significantly when entropy was taken into account. Still in disagreement with the theoretical results, the activation energy for isobutane was significantly lower than that for linear hydrocarbons [8,9] (see Table 1). This discrepancy may indicate that in this case the direct mechanism is not the proper one, and other alternatives, such as the mediated bimolecular mechanism suggested by Sommer et al. [8], should be considered. We address this issue in Section 5.

In agreement with our calculations and with the results of other theoretical studies [33,34,36], the activation energies for H-exchange involving either CH_3 or CH_2 groups of propane were found to be similar within the limits of experimental error (see Table 1). Thus the observed regioselectivity of propane cannot be explained in terms of activation energy differences. For isobutane, theory predicts no or only a very modest difference in the activation energies for reactions involving either methyl or methine groups. In contrast, NMR experiments performed by Sommer et al. [8] and by Truitt et al. [9] clearly show that the methine group is much less active for proton exchange. To explain this experimental fact, a simple potential-energy analysis is obviously not sufficient, and entropic effects must be taken into account.

4. Thermal effects

4.1. Interaction of alkanes with the Brønsted acid site

First, we propose a qualitative analysis of the effects at the origin of the observed regioselectivity for two different hydrocarbons, propane [4–6] and isobutane [8,9]. Ab initio MD simulations were performed over a time span of 100 ps at a temperature of 300 K. As we showed in Section 3.1, the calculated potential-energy barriers for proton exchange were >100 kJ/mol for all alkanes; therefore, the probability that the reaction occurs during the simulation period of 100 ps is negligible.

For the reaction to occur at least one carbon atom must get close enough to the site, that is, the bridging OH group. As described in Section 3.1, the distance between the acid proton and the nearest carbon atom is shorter than 3 Å in all adsorption complexes (see parameter r_1 in Table 2). Because

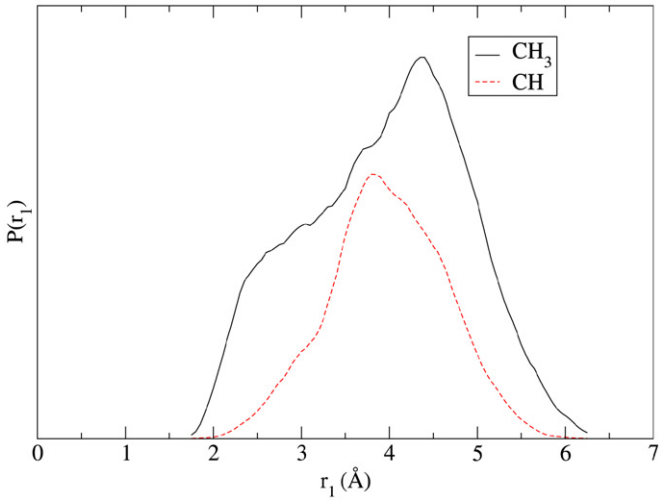

Fig. 3. Probability distribution for the distance between the hydrogen atom in the Brønsted acid site and the carbon atom in the methyl (—) and methylene (- - -) groups of propane.

the adsorption energy of the alkane at the Brønsted acid site is only ∼10–15 kJ/mol, the adsorption complexes can easily collapse. For propane, the probability of finding a configuration in which the shortest carbon-proton distance shorter than 3 Å is ∼45%. This means that a propane molecule can easily move and rotate in the chabazite cavity during most of the simulation period. Because of the quite frequent oscillations between adsorbed ($r_1 < 3$ Å) and desorbed ($r_1 > 3$ Å) states, we could efficiently sample probabilities of creating different adsorption complexes. Probability distribution functions for the distance r_1 in two different adsorption complexes of propane, interacting either via a methyl ($P^{CH_3}(r_1)$) or a methylene ($P^{CH_2}(r_1)$) group with the bridging OH group in chabazite, are shown in Fig. 3. We define the probability of creating an adsorption complex p_{ads} as

$$p_{ads} = \int_0^{r_1^{eff}} P(r_1)\, dr_1, \tag{1}$$

where r_1^{eff} is the largest r_1 allowed for a configuration to be still considered an adsorption complex. Taking $r_1^{eff} = 3$ Å, we find that the probability for propane to adsorb via a CH_3 group, ($p_{ads}^{CH_3}$), is about seven times higher than that for adsorption via a CH_2 group, ($p_{ads}^{CH_2}$). For $r_1^{eff} = 2.8$ Å the ratio of $p_{ads}^{CH_3}$ and $p_{ads}^{CH_2}$ is 9, whereas for $r_1^{eff} = 2.6$ Å, it is 17.

The higher adsorption probability via methyl groups is due to two factors: (i) There are two CH_3 groups in propane, compared to only one CH_2 group. (ii) A steric effect: although the two terminal CH_3 groups can relatively easily approach the bridging OH group, the central CH_2 group can interact efficiently with the Brønsted acid site only if the molecule is oriented in such a way that repulsive interactions between zeolite framework and the CH_3 groups are avoided.

Both of these effects are even more pronounced for isobutane, because contact between the methine group and the Brønsted site is more difficult due to the presence of three methyl

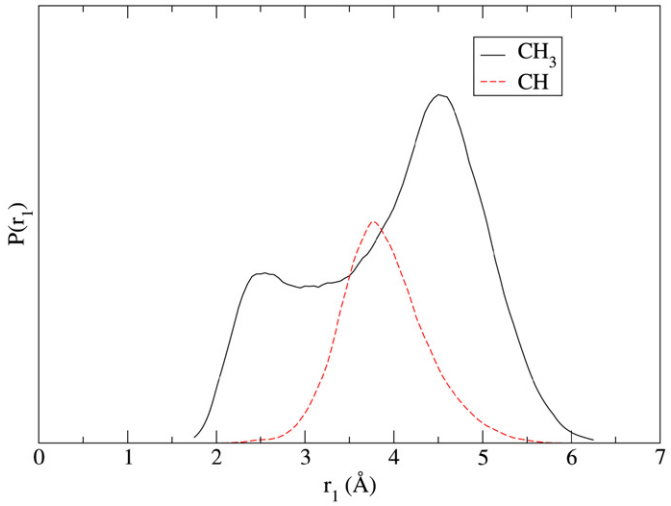

Fig. 4. Probability distribution for the distance between the hydrogen atom in the Brønsted acid site and the carbon atom in the methyl (—) and methine (- - -) groups of isobutane.

groups. As shown in Fig. 4, the probability that the methine group be close enough to the proton to form an adsorption complex is much lower than that for the methyl groups. Using Eq. (1), we find that the ratio $p_{\text{ads}}^{\text{CH}_3}/p_{\text{ads}}^{\text{CH}} = 35$ for $r_1^{\text{eff}} = 3.0$ Å and it increases to 233 for $r_1^{\text{eff}} = 2.6$ Å. This result clearly shows that even though the interaction energies calculated for complexes bound via methine and methyl groups are the same (∼10 kJ/mol, see Table 3), the joint probability of creating the adsorption complex followed by the proton exchange is strongly reduced by entropic effects.

Our analysis predicts a significant difference in the activity of different functional groups in propane and isobutane. We show that the activity of the methine group in isobutane is suppressed already at the very first stage of reaction, during the formation of an adsorption complex. Differences in adsorption probabilities between methyl and methine groups are of two orders of magnitude, which explains why H-exchange via a methine group has never been observed [8,9]. On the other hand, although the probability that the propane adsorbs via the methylene group is also decreased due to entropy, it remains nonnegligible. This result is in agreement with the experimental fact that both functional groups of propane are active in H-exchange, with the rate of reaction for the methyl group being larger by factor of three [4–6]. Because the regioselectivity is due to mainly steric effects, it is expected that the activity of various hydrocarbon functional groups strongly depends on the local geometry of the zeolite framework as well.

4.2. Free-energy reaction profile

A popular method for estimating the free-energy barrier of a reaction is based on harmonic transition state theory [40]. In fact, harmonic transition state theory is able to provide reasonable estimates for the entropic contribution only if the following two conditions are fulfilled: (i) All vibrational degrees of freedom can be represented by harmonic oscillators, and (ii) the free-energy minima and saddle points are close to the corresponding critical points on the potential-energy landscape. Both of these criteria are satisfied only for strongly bound complexes. For weakly adsorbed systems, such as those studied here, none of these conditions is fulfilled. Obviously, soft degrees of freedom, such as hindered translations and rotations, cannot be represented by harmonic oscillators. Even worse, as we show later, the potential-energy minima do not coincide with the free-energy minima. Thus simple harmonic transition theory is not useful in this case and more sophisticated methods must be used.

In this work, we calculate free-energy barriers in two steps,

$$\Delta A_{\text{fM}\to\text{fTS}} = \Delta A_{\text{fM}\to\text{fR}} + \Delta A_{\text{fR}\to\text{fTS}}. \tag{2}$$

The first term on the right side corresponds to the free-energy change due to the transition from the free-energy minimum (fM) to a reference state (fR) chosen such that its probability $p(\text{fR})$ is sufficiently high to be determined using standard MD simulations. The free-energy difference $\Delta A_{\text{fM}\to\text{fR}}$ then can be calculated via

$$\Delta A_{\text{fM}\to\text{fR}} = -RT\ln\bigl(p(\text{fR})/p(\text{fM})\bigr). \tag{3}$$

The second term in Eq. (2), $\Delta A_{\text{fR}\to\text{fTS}}$, represents the free-energy change due to the transition from the reference configuration fR to the free-energy transition state fTS. If $\Delta A_{\text{fR}\to\text{fTS}} > RT$, this process is a rare event, and thus its probability $p(\text{fTS})$ cannot be sampled efficiently using standard MD techniques. We determine this term using the thermodynamical integration as described in Appendix A.

4.2.1. Free-energy minima

To calculate the term $\Delta A_{\text{fM}\to\text{fR}}$ in Eq. (2), first the free-energy minimum must be located. The probability of a state defined by the parameters $\boldsymbol{\xi} = \{\xi_i; i = 1,\ldots,r\}$ is given by

$$P(\xi) = \frac{\int dx\,dp\,\prod_{i=1}^{r}\delta(\xi_i(x)-\xi_i)\,e^{-H(x,p)/kT}}{\int dx\,dp\,e^{-H(x,p)/kT}}. \tag{4}$$

We note that only four parameters, two C···H and two O···H distances, undergo significant changes during the reaction. The four parameters r_1–r_4 defined in Fig. 2 thus form the basis for the definition of a free-energy reaction coordinate. Because the parameters r_2 and r_3 correspond to the C–H and O–H chemical bonds, respectively, they simply oscillate around their thermal averages $\langle r_2\rangle$ and $\langle r_3\rangle$, but do not correlate with the other two parameters during the standard MD simulation. Hence the problem of finding the free-energy minima reduces to two dimensions. In principle, we can define parameters r_1 to r_4 for each of the four CH_n groups in isobutane and analyze them separately. However, on the basis of symmetry arguments, we can consider to a good approximation the three carbon atoms and the nine hydrogen atoms equivalent. Thus when analyzing the probability distribution for methyl groups, only the shortest distance between a C atom in any of the CH_3 groups and the proton (r_1), the shortest distance between the framework oxygen atom O2 (see Fig. 2), as well as a H atom in that CH_3 group which is closest to the proton, is considered.

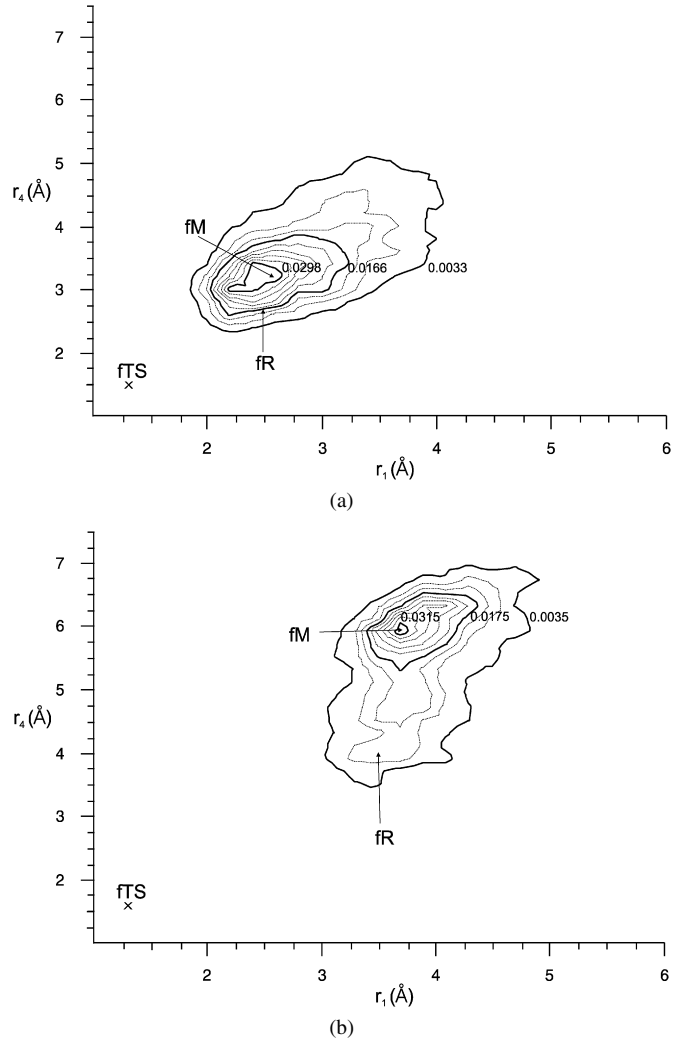

Fig. 5. Two-dimensional distribution functions $P(r_1, r_4)$ for the methyl group (a) and for the methine group (b) of isobutane, as defined in the text. Interatomic distances r_1 and r_4 are as defined in Fig. 2. Values of $P(r_1, r_4)$ for solid contours are shown. Positions of free-energy minima (fM), reference points (fR) and transition states (fTS) are marked.

The two-dimensional probability distribution functions $P(r_1, r_4)$ for the methyl and the methine groups are shown in Fig. 5. The points with the highest probability correspond to the free-energy minima (fM). For methyl groups, the most likely configuration is found at $r_1 = 2.6 \pm 0.1$ Å, $r_2 = \langle r_2 \rangle = 1.110 \pm 0.001$ Å, $r_3 = \langle r_3 \rangle = 0.985 \pm 0.001$ Å, and $r_4 = 3.2 \pm 0.1$ Å with a probability of ∼0.030. Comparing these parameters with those reported in Table 2 for the adsorption of isobutane via a methyl group, it can be concluded that, although parameters $r_1 - r_3$ in the potential- and the free-energy minima are the same within the error bar, the parameter r_4 differs by ∼0.5 Å. Thus, creating a configuration similar to the adsorption complex identified using potential-energy minimization requires a certain amount of work. This work is quite minimal (∼2 kJ/mol) for a complex bound via a methyl group.

Similarly, for the methine group, the maximum probability is found at $r_1 = 3.7 \pm 0.1$ Å, $r_2 = \langle r_2 \rangle = 1.115 \pm 0.001$ Å, $r_3 = \langle r_3 \rangle = 0.985 \pm 0.001$ Å, and $r_4 = 5.9 \pm 0.1$ Å with $P(r_1, r_4) =$ 0.031. Obviously, this configuration is markedly different from the corresponding potential-energy minimum. In particular, the parameters r_1 and r_4 are larger by ∼1.3 and 3.2 Å, respectively. In fact, the probability of finding the potential-energy minimum is so low that it cannot be sampled by a standard MD simulation. Thus, the work needed to bring the methine group close to the proton and a framework O atom contributes significantly to the free-energy profile of the reaction.

Table 5
Interatomic distances (Å) in potential- and free-energy transition states for direct proton exchange between primary (tertiary) carbon atom of isobutane and proton at Brønsted acid site in chabazite. Parameters $r_1 - r_4$ are defined in Fig. 2

	Primary C				Tertiary C			
	r_1	r_2	r_3	r_4	r_1	r_2	r_3	r_4
pTS	1.26	1.31	1.48	1.47	1.26	1.38	1.60	1.50
fTS	1.26	1.29	1.49	1.51	1.28	1.33	1.66	1.62

To calculate the first term on the right side of Eq. (2), suitable reference points, fR, must be defined, for which the probability $P(r_1, r_4)$ is sufficiently high to allow efficient sampling using standard MD simulation. For adsorption via a methyl group, fR is defined using the parameters $\xi(CH_3) = \{r_1, r_2, r_3, r_4\} = \{2.51$ Å, 1.11 Å, 0.98 Å, 2.71 Å$\}$ (see Fig. 5). Using Eq. (3), we calculate the free-energy contribution $\Delta A_{fM \to fR}$ of ∼2 kJ/mol. Similarly, parameters $\xi(CH) = \{r_1, r_2, r_3, r_4\} = \{3.49$ Å, 1.11 Å, 0.98 Å, 4.00 Å$\}$ define the reference configuration fR for the adsorption complex bound via the methine group with $\Delta A_{fM \to fR} = \sim 3$ kJ/mol.

4.2.2. Free-energy transition states

Following Ziegler and Fleurat-Lessard [27], we located the free-energy transition states (fTS) by calculating the free-energy gradients defined by Eq. (A.12), and using the partitioned rational function optimization (p-RFO) method [41]. Each geometry optimization was started from the potential-energy transition state configuration (pTS) and from the corresponding Hesse matrix. During the optimization, the Hesse matrix was updated using a weighted combination [45] of Powell symmetric-Broyden (PBS) [42,43] and symmetric rank-one (SR1) [44] formulae. Because ab initio MD simulations for large systems are extremely demanding, a rather loose optimization criterion was used. The free-energy optimization was terminated if all gradients were <0.10 eV/Å. The free-energy gradients were evaluated for a trajectory of 10 ps, where the initial period of 2 ps was used for equilibration, and the corresponding gradients were not included in thermal averages of (Eq. (A.12)).

The four parameters $r_1 - r_4$ defining potential- and free-energy TS configurations are compared in Table 5. Because of the modest simulation temperature, the parameters for fTS are rather similar to those for pTS configurations, the difference being a few hundredths of Å.

4.2.3. Free-energy barriers

Having identified the free-energy transition state, Eq. (A.1) was used to calculate the free-energy difference between the transition state fTS and the reference configuration fR as de-

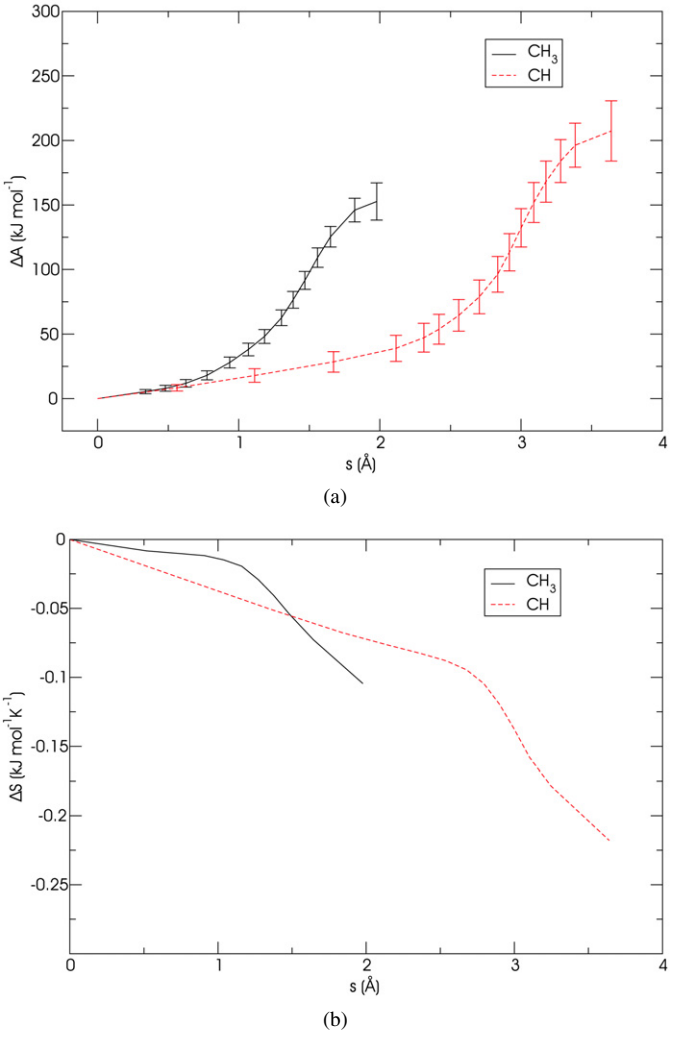

Fig. 6. Free-energy profiles along the reaction path (a) and the corresponding entropy change (b) for proton exchange between the methyl (CH_3) or methine (CH) groups of isobutane and the OH group of acidic chabazite. As reference points, configurations fR ($s = 0$) as shown in Fig. 5 are chosen. Points with the highest value of $\Delta A_{\mathrm{fR}\to\mathrm{fTS}}$ correspond to free-energy transition states fTS.

fined in Section 4.2.1. We integrated Eq. (A.1) along the parameterized intrinsic reaction path [46,47] (IRC) determined on the potential-energy surface. We assume that at a relatively low simulation temperature, the potential-energy IRC is rather similar to its free-energy analog. Because in principle, $\Delta A_{1\to 2}$ depends only on states 1 and 2 and not on the path itself, the integration path can be chosen arbitrarily. However, the transition state is not necessarily a maximum on the resulting free-energy profile. As in the fTS calculations, gradients were sampled for 8 ps after an equilibration period of 2 ps.

The calculated free-energy profiles for the transition fR → fTS as function of the path length $s(x)$ (defined in Appendix B) are shown in the upper panel of Fig. 6. Adding terms $\Delta A_{\mathrm{fM}\to\mathrm{fR}} + \Delta A_{\mathrm{fR}\to\mathrm{fTS}}$ according to Eq. (2), we find the free-energy barriers of 155 ± 14 and 210 ± 23 kJ/mol for methyl and methine groups, respectively. These values are significantly larger than the corresponding potential-energy differences between saddle points and minima determined by relaxations with the same plane-wave cutoff as used in the MD simulations (112 and 125 kJ/mol, respectively). It is obvious that in this case ignoring entropic effects leads to a serious underestimation of reaction barriers. A similar trend is expected for the other hydrocarbons considered in this study. Furthermore, if entropy is taken into account, the difference between barriers for proton exchange involving methyl and methine groups increases significantly. The entropy contribution can be calculated using equation

$$\Delta S_{\mathrm{fR}\to\mathrm{fTS}} = \frac{\Delta U_{\mathrm{fR}\to\mathrm{fTS}} - \Delta A_{\mathrm{fR}\to\mathrm{fTS}}}{T}. \tag{5}$$

The internal energy U_{ξ^*} can be approximated by the average potential-energy $\langle E\rangle_{\xi^*}$ calculated on the basis of constrained MD simulations using Eq. (A.3). The change of entropy along a path connecting states fR and fTS is shown in the lower panel of Fig. 6. The term $\Delta S_{\mathrm{fR}\to\mathrm{fTS}}$ is negative for proton exchange. This is expected because isobutane, which interacts only weakly with the zeolite OH group in state fR, becomes strongly bound in the fTS state and thus loses entropy on the transformation fR → fTS.

ΔS as function of path length s shows some common features for both reactions. Initially, entropy decreases rather slowly. Indeed, the region with a slow decrease of ΔS (interval $s = 0$ to 1.1 for the methyl group and $s = 0$ to 2.7 for the methine group) corresponds to a translation of the isobutane molecule toward the bridging OH group. According to our analysis in Section 4.2.1, bringing the methine group sufficiently close to the bridging OH groups requires more work than for the methyl group. Because the potential-energy change for this process is rather modest in both cases, this work is required to compensate the loss of entropy. Thus, isobutane looses entropy when forming a complex adsorbed via the methine group. The region with larger negative slope of ΔS corresponds to bond breaking, that is, to the chemical reaction itself. It is remarkable that the entropy change for this process is very similar for both methine and methyl groups.

In transition-state theory, the ratio between the rate constants for proton exchange via a methyl group ($k(\mathrm{CH_3})$) or the methane group ($k(\mathrm{CH})$) can be expressed as

$$\frac{k(\mathrm{CH_3})}{k(\mathrm{CH})} \approx e^{-(\Delta A^{\ddagger}(\mathrm{CH_3}) - \Delta A^{\ddagger}(\mathrm{CH}))/kT}. \tag{6}$$

Using this equation, we find that proton exchange with a methyl group is about nine orders of magnitude faster than that with the reaction involving a CH group. Thus, proton exchange via the methine group is very unlikely.

5. Mediated mechanism

For the proton-exchange between isobutane and an acid site, Sommer et al. [8] proposed an alternative mechanism shown in Scheme 2. In this mechanism, a methylpropene molecule plays the role of a co-catalyst. Methylpropene is supposed to be present in the feedstock either as an impurity or as a byproduct created in previous reaction steps. Due to its higher proton affinity, methylpropene is more easily protonated than isobutane on interaction with a Brønsted acid site and forms a *tert*-

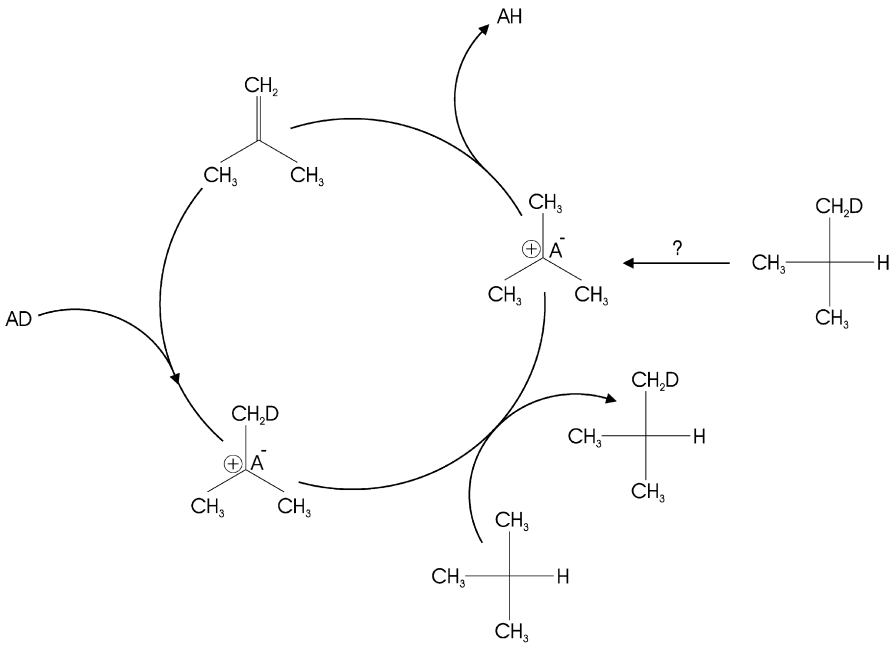

Scheme 2.

butyl cation. The tertiary carbon atom in the *tert*-butyl cation interacts with the methine group of the isobutane, and eventually a hydride transfer occurs. The *tert*-butyl cation created in this reaction can either enter another catalytic cycle or become deprotonated on interaction with a framework O atom to form neutral methylpropene and a Brønsted acid site.

Similar to the direct mechanism, we first identify minima and saddle points for this reaction. We consider a typical experimental setup in which the hydrogen atom at the bridging OH group is initially exchanged for deuterium, but all hydrogen atoms at hydrocarbons are protium isotopes. In the initial configuration, R1, methylpropene forms an adsorption complex with the bridging OD group of the zeolite (see Fig. 7). The isobutane molecule is too far from the OD group to form an adsorption complex. In the first reaction step, proton transfer occurs from the Brønsted acid site to methylpropene. In the transition state, deuterium is about midway between the framework oxygen atom, and the carbon atom in the methylene group of methylpropene (see Fig. 8 TS1). The calculated activation energy for this reaction step is 27 kJ/mol. In the reaction intermediate R2, the *tert*-butyl cation is stabilized by interaction with the methine group of isobutane, and a complex with a shared hydride is created. Such a configuration has been reported previously in a slightly different context [48]. The stability of this complex is almost the same as that of the initial configuration R1, with a difference in potential energy of only 2 kJ/mol (see Fig. 9). The formation of a *tert*-butyl cation in the reaction intermediate also explains why the mediated mechanism is not effective for linear hydrocarbons, where tertiary cations cannot be formed and secondary and primary cations are unstable.

From this point on, the reaction proceeds through the same steps as described so far, but in reverse order; that is, the complex with a shared hydride collapses to form isobutane and a *tert*-butyl cation (TS2), which deprotonates on interaction with the framework O atom next to the Al atom to form methylpropene physisorbed at a bridging OH group (R3). In the final configuration, R3, deuterium is located in the methyl group of isobutane, whereas the bridging OH group contains protium. Thus, in effect, only a H/D exchange of the methyl group of isobutane with the Brønsted acid site is observed in the experiments, although the methine groups also take part in the reaction in the mediated mechanism. The mediated mechanism is thus consistent with the experimentally observed regioselectivity between methyl and methine groups of isobutane [8,9].

Because configurations R1 and R3 differ only in terms of the positions of methylpropene and isobutane in the zeolite and by the position of deuterium, the calculated potential energy for R3 is almost the same as that for R1, and the heat of reaction is negligible.

The mediated mechanism involves two reaction steps with activation energies of ∼25 kJ/mol, which are considerably lower compared with the barrier calculated for the direct mechanism (see Table 3). On the other hand, the activation energies for the reverse reactions are also very low, and thus at first sight, the back-reaction seems as likely as the forward reaction. Once again, the entropy effect is important. Because initially the deuterium can sit at any of the four oxygen atoms close to the aluminum atom, there are four different realizations of state R1, but only one realization of state R2. Because of the stability of configuration R2 relative to states R1 and R3, it is reasonable to assume that any of the 17 hydrogen atoms at the methyl groups in R2 can jump with the same probability to any of the four framework oxygen atoms close to the aluminum atom, leading to 68 different realizations of state R3. Altogether, one single configuration R2 is in thermal equilibrium with four realizations of state R1 and with 68 realizations of states R3. Thus, chemical equilibrium is strongly shifted toward product configurations R3.

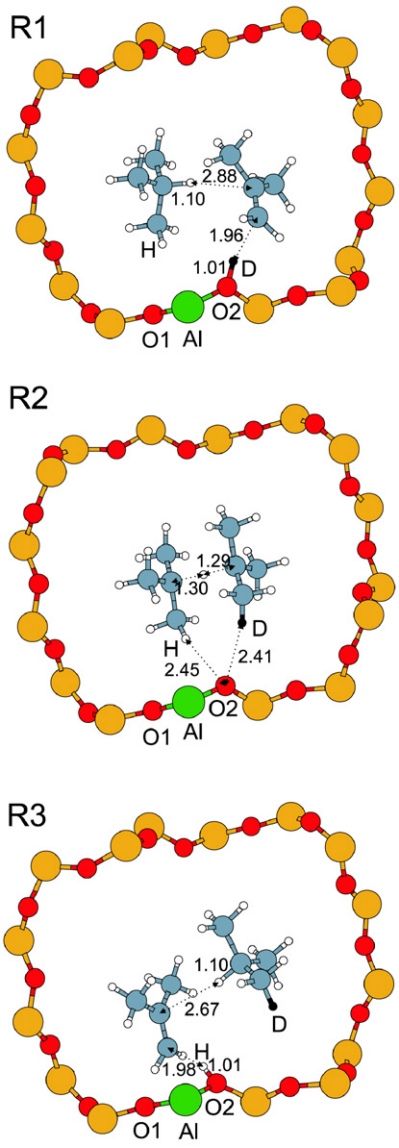

Fig. 7. Reaction intermediates for the mediated mechanism of proton exchange reaction: methylpropene physisorbed at the deuterated Brønsted acid site, linked via a weak hydrogen bond to isobutane (R1); 'shared hydride complex' between the *tert*-butyl cation and isobutane, mediated by a hydrogen atom from the methine group (R2); deuterated isobutane and methylpropene physisorbed at the Brønsted acid site (R3). Selected interatomic distances are in Å.

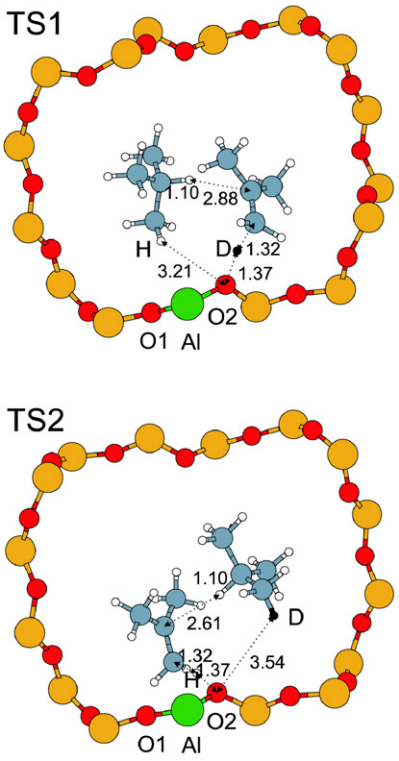

Fig. 8. Transition states for the mediated mechanism of proton exchange reaction: TS1—formation of a *tert*-butyl cation (reaction R1 → R2); TS2—deprotonation of isobutane (reaction R2 → R3). Selected interatomic distances are in Å.

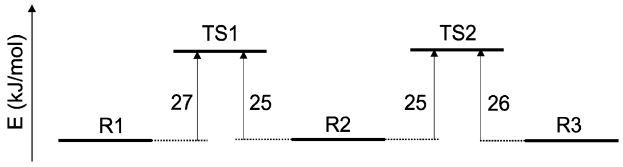

Fig. 9. Reaction energy diagram for the mediated mechanism of proton exchange of isobutane over acidic chabazite. Structures corresponding to stable reaction intermediates (R1, R2, and R3) and transition states (TS1 and TS2) are displayed in Figs. 7 and 8.

6. Conclusion

We have investigated proton exchange between short hydrocarbons and acidic chabazite using periodic DFT calculations. As we have shown, the activation energies for the direct mechanism are essentially independent of the length of the hydrocarbon chain of short alkanes. This result is in agreement with available experimental data [4,6,7,39]. For larger hydrocarbons such as hexane, however, the repulsive interactions between the zeolite framework and the hydrocarbon would certainly come into play. This effect would be expected to destabilize transition structures more than the adsorption complex, and consequently, the activation energy should increase.

The experimentally observed regioselectivity between methyl and methylene groups in propane [4–6] and methyl and methine groups of isobutane [8,9] cannot be understood on the basis of a potential-energy analysis alone. For the former reactions, the calculated potential-energy barriers are almost the same; for the latter, the difference is only ∼12 kJ/mol. We have shown that the entropy contribution is the decisive factor in both cases. Mainly due to steric reasons, the probability of adsorption of propane via the methylene group is ∼17 times lower than that of adsorption via a methyl group. This effect is even stronger for isobutane where the probability of the adsorption complex bound via the CH group is ∼233 times lower compared with adsorption via a methyl group. This entropy contribution leads to a much higher free-energy barrier for proton-exchange via the methine group. On the basis of our MD simulations, it is estimated that the reaction rate for proton exchange via a methyl group is about nine orders of magnitude higher compared with reaction via the methine group.

The calculated potential barriers for direct proton-exchange reactions of isobutane are significantly higher compared with those for linear hydrocarbons. At first sight, this seems to be in disagreement with the experiments of Sommer et al. [8] and Truitt et al. [9], who found significantly lower apparent activation energies than for linear hydrocarbons. A possible explanation for this disagreement could be that a different reaction mechanism is active for the proton exchange of isobutane. We have studied the mechanism suggested by Sommer et al. [8] in which the reaction is mediated by methylpropene present in the feedstock. We have shown that proton-exchange proceeds via two activated steps, with significantly lower barriers than for the direct mechanism. Although the barriers for forward and backward reaction modes are about the same, due to entropy effects, the reaction equilibrium is shifted toward the products. If methylpropene molecules are present in the feed at sufficient concentration, then the mediated mechanism should be dominant. Due to the formation of a tertiary carbocation as a reaction intermediate, it can operate only for branched hydrocarbons. On the other hand, the difficulty with the mediated mechanism is that the concentration of methylpropene does not increase during the proton-exchange reaction, and thus the transport to bridging O–D sites might be the slowest reaction step. A study of hydrocarbon diffusion in zeolites is beyond the scope of this paper and would be better answered by experiments. A measured correlation between the reaction rate and the concentration of methylpropene would provide strong evidence in favor of the mediated mechanism.

Acknowledgments

This work was supported by the Austrian Science Fund under project P17020 and by the Institut Français du Pétrole. The authors thank the staff at the Computing Center of Vienna University for the use of their facilities and Professor Ch. Dellago for helpful discussions.

Appendix A. Free-energy gradients

In this appendix we briefly describe our strategy for the calculation of free-energy gradients, following Refs. [24–27]. If two states 1 and 2 are characterized by two vectors of internal parameters $\boldsymbol{\xi}(1) = \{\xi_i(1); i = 1, \ldots, r\}$ and $\boldsymbol{\xi}(2) = \{\xi_i(2); i = 1, \ldots, r\}$, respectively, then the free-energy difference between these two states ($\Delta A_{1\to 2}$) can be calculated by integrating the free-energy gradient along a path connecting states 1 and 2,

$$\Delta A_{1\to 2} = \int_{\xi(1)}^{\xi(2)} \left(\frac{\partial A}{\partial \xi}\right)_{\xi^*} d\xi. \tag{A.1}$$

The free energy along the reaction path $A(\xi^*)$ is related to the partition function $Q(\xi^*)$ by $A(\xi^*) = -RT \ln[Q(\xi^*)]$. Therefore, calculating the free-energy gradient first requires evaluating the derivative of the partition function, $\frac{\partial Q}{\partial \xi}$. The partition function is defined by

$$Q(\xi^*) = \int dq \int dp_q dp_\xi \exp(-\beta H), \tag{A.2}$$

where the dynamical variables of the Hamiltonian have been split into the active coordinates $\boldsymbol{\xi} = \{\xi_i; i = 1, \ldots, r\}$ defining the reaction path, the inactive coordinates $\mathbf{q} = \{q_i; i = 1, \ldots, 3N - r\}$, and the associated momenta p_ξ and p_q. In the MD simulations, the reaction coordinates are constrained to remain constant and equal to ξ^*, which requires the additional constraint $\dot{\xi} = 0$. Therefore, during the MD simulation p_ξ is not sampled; constrained ensemble averages over a quantity $\mathcal{O}$ are evaluated as

$$\langle \mathcal{O} \rangle_{\xi^*} = \frac{\int dq \int dp_q \mathcal{O} \exp(-\beta H^c_{\xi^*})}{\int dq \int dp_q \exp(-\beta H^c_{\xi^*})}, \tag{A.3}$$

with the Hamiltonian

$$H^c_{\xi^*} = \frac{1}{2}\mathbf{p}_q^t \mathbf{X} \mathbf{p}_q + V(\mathbf{q}, \xi). \tag{A.4}$$

The mass-metric tensor X is defined as

$$X_{\alpha,\beta} = \sum_{i=1}^{i=3N} \frac{1}{m_i} \frac{\partial q_\alpha}{\partial x_i} \frac{\partial q_\beta}{\partial x_i}, \quad \alpha = 1, \ldots, 3N - r, \quad \beta = 1, \ldots, 3N - r. \tag{A.5}$$

The unconstrained average is

$$\langle \mathcal{O} \rangle = \frac{\int dq\, d\xi \int dp_q\, dp_\xi \mathcal{O} \exp(-\beta H)}{\int dq\, d\xi \int dp_q\, dp_\xi \exp(-\beta H)}, \tag{A.6}$$

whereby the unconstrained and constrained Hamiltonians are related via

$$H = H^c_{\xi^*} + \frac{1}{2}\left(\mathbf{p}_\xi^t \mathbf{Y} \mathbf{p}_q + \left(\mathbf{p}_\xi^t \mathbf{Y} \mathbf{p}_q\right)^t + \mathbf{p}_\xi^t \mathbf{Z} \mathbf{p}_\xi\right). \tag{A.7}$$

The mass-metric tensors Y and Z are defined as

$$Y_{\alpha,\beta} = \sum_{i=1}^{i=3N} \frac{1}{m_i} \frac{\partial \xi_\alpha}{\partial x_i} \frac{\partial q_\beta}{\partial x_i}, \quad \alpha = 1, \ldots, r, \quad \beta = 1, \ldots, 3N - r \tag{A.8}$$

and

$$Z_{\alpha,\beta} = \sum_{i=1}^{i=3N} \frac{1}{m_i} \frac{\partial \xi_\alpha}{\partial x_i} \frac{\partial \xi_\beta}{\partial x_i}, \quad \alpha = 1, \ldots, r, \quad \beta = 1, \ldots, r. \tag{A.9}$$

Following Carter et al. [24], constrained and unconstrained ensemble averages are related through a "blue moon" correction,

$$\langle \mathcal{O} \rangle = \frac{\langle \mathcal{O} Z^{-1/2} \rangle_{\xi^*}}{\langle Z^{-1/2} \rangle_{\xi^*}}, \tag{A.10}$$

where the angular brackets $\langle \ldots \rangle_{\xi^*}$ denote conditional thermal averages with constrained components of the vector ξ.

To constrain the system to remain on the reaction path during the MD simulation, a modified Lagrangian with the Lagrange multipliers $\lambda = \{\lambda_{\xi 1}, \ldots, \lambda_{\xi r}\}$ associated with the reaction coordinate is used,

$$\mathcal{L}^*(\mathbf{x}, \boldsymbol{\xi}, \dot{\mathbf{x}}) = \mathcal{L}(\mathbf{x}, \dot{\mathbf{x}}) + \sum_{i=1}^{i=r} \lambda_{\xi i}\left(\xi_i(\mathbf{x}) - \xi_i\right). \tag{A.11}$$

In our simulations, we used the SHAKE algorithm [49] to determine the Lagrange multipliers. It can be shown [25–27] that the free-energy gradients $(\frac{\partial A}{\partial \xi_k})_{\xi^*}$ can be calculated using the Lagrange multipliers via formula

$$\left(\frac{\partial A}{\partial \xi_k}\right)_{\xi^*} = \frac{1}{\langle |\mathbf{Z}|^{-1/2}\rangle_{\xi^*}} \left\langle |\mathbf{Z}|^{-1/2} \left[-\lambda_{\xi_k} + k_B T \sum_{j=1}^{j=r} (\mathbf{Z}^{-1})_{kj} \sum_{i=1}^{i=3N} \frac{1}{m_i} \frac{\partial \xi_j}{\partial x_i} \frac{\partial |\mathbf{Z}|}{\partial x_i} \right] \right\rangle_{\xi^*}. \quad \text{(A.12)}$$

Appendix B. Reaction path length

The reaction path is represented by sequence of $N+1$ configurations characterized by vectors $\xi(0), \ldots, \xi(N)$ connecting the free-energy transition state fTS and reference configuration fR. Setting $\xi(0) = \xi(\text{fR})$ and $\xi(N) = \xi(\text{fTS})$, the length of reaction path is defined as

$$s\big(\boldsymbol{\xi}(0)\big) = 0, \quad \text{(B.1)}$$

$$s\big(\boldsymbol{\xi}(i+1)\big) = \sum_{j=0}^{i} \big|\boldsymbol{\xi}(j+1) - \boldsymbol{\xi}(j)\big|, \quad i = 0, \ldots, N-1. \quad \text{(B.2)}$$

Appendix C. Integration formula and statistical error estimate

The free-energy difference ΔA given by the integral in Eq. (A.1) was calculated using the trapezoid rule as

$$\Delta A = \frac{1}{2}\mathbf{f}(0)\cdot\big(\boldsymbol{\xi}(1) - \boldsymbol{\xi}(0)\big) + \frac{1}{2}\sum_{i=1}^{N-1} \mathbf{f}(i)\cdot\big(\boldsymbol{\xi}(i+1) - \boldsymbol{\xi}(i-1)\big) + \frac{1}{2}\mathbf{f}(N)\cdot\big(\boldsymbol{\xi}(N) - \boldsymbol{\xi}(N-1)\big) + \mathcal{O}\big(\Delta\xi^2\big), \quad \text{(C.1)}$$

where we use the shorthand notation $\mathbf{f}(i) = \{(\frac{\partial A}{\partial \xi_j})_{\xi(i)}; j = 1, \ldots, r\}$ for the free-energy gradients and replace indices fR and fTS by 0 and N, respectively. In our case, configurations $\boldsymbol{\xi}(0), \ldots, \boldsymbol{\xi}(N-1)$ can be chosen arbitrarily, therefore only the error due to the convergence of the gradients $\epsilon_{f(i)_j}$ contributes to the statistical error of ΔA. The transition state configuration $\xi(N)$, on the other hand, is determined with an uncertainty $\epsilon_{\xi(N)_j}$, but by definition, in the transition state, all gradients vanish; thus, $\epsilon_{f(N)_j} = 0$ for all components $i = 1, \ldots, r$. The statistical error in the free-energy difference $\epsilon_{\Delta A}$ due to an imperfect convergence of the free-energy gradients is hence given by

$$\epsilon_{\Delta A} = \frac{1}{2}\sum_{j=1}^{r} \epsilon_{f(0)_j} \big|\xi(1)_j - \xi(0)_j\big| + \frac{1}{2}\sum_{i=1}^{N-1}\sum_{j=1}^{r} \epsilon_{f(i)_j} \big|\xi(i+1)_j - \xi(i-1)_j\big| + \frac{1}{2}\sum_{j=1}^{r} \epsilon_{\xi(N)_j} \big|f(N-1)_j\big|. \quad \text{(C.2)}$$

The statistical error due to the use of the trapezoidal rule for numerical integration is of order $\mathcal{O}(\Delta\xi^2)$ and cannot be expressed without explicit knowledge of the form of integrand. Note, however, that this error can be significantly reduced by using a sufficiently dense integration grid, especially in regions in which the integrand changes rapidly.

References

[1] G.J. Kramer, R.A. van Santen, C.A. Emels, A.K. Nowak, Nature 363 (1993) 529.
[2] J. Engelhardt, J. Valyon, React. Kinet. Catal. Lett. 74 (2001) 217.
[3] J. Valyon, J. Engelhardt, D. Kalló, M. Hegedüs, Catal. Lett. 82 (2002) 29.
[4] A.G. Stepanov, H. Ernst, D. Freude, Catal. Lett. 54 (1998) 1.
[5] A.G. Stepanov, S.S. Arzumanov, M.V. Luzgin, H. Ernst, D. Freude, V.N. Parmon, J. Catal. 235 (2005) 1.
[6] S.S. Arzumanov, S.I. Reshetnikov, A.G. Stepanov, V.N. Parmon, D. Freude, J. Phys. Chem. B 109 (2005) 1.
[7] J.A. Lercher, R.A. van Santen, H. Vinek, Catal. Lett. 27 (1994) 91.
[8] J. Sommer, D. Habermacher, R. Jost, A. Sassi, A.G. Stepanov, M.V. Luzgin, D. Freude, H. Ernst, J. Martens, J. Catal. 181 (1999) 265.
[9] M.J. Truitt, S.S. Toporek, R. Rovira-Truitt, J.L. White, J. Am. Chem. Soc. 128 (2006) 1847.
[10] Y. Jeanvoine, J.G. Ángyán, G. Kresse, J. Hafner, J. Phys. Chem. B 102 (1998) 5573.
[11] S.I. Zones, R.A. Van Nostrand, Zeolites 8 (1988) 166.
[12] G. Kresse, J. Hafner, Phys. Rev. B 48 (1993) 13115.
[13] G. Kresse, J. Hafner, Phys. Rev. B 49 (1994) 14251.
[14] G. Kresse, J. Furthmüller, Comput. Mater. Sci. 6 (1996) 15.
[15] G. Kresse, J. Furthmüller, Phys. Rev. B 54 (1996) 11196.
[16] J.P. Perdew, J.A. Chewary, S.H. Vosko, K.A. Jackson, M.R. Pedersen, D.J. Singh, C. Fiolhais, Phys. Rev. B 46 (1992) 6671.
[17] J.P. Perdew, Y. Wang, Phys. Rev. B 45 (1992) 13244.
[18] P.E. Blöchl, Phys. Rev. B 50 (1994) 17953.
[19] G. Kresse, D. Joubert, Phys. Rev. B 59 (1999) 1758.
[20] G. Henkelman, H. Jónsson, J. Chem. Phys. 111 (2000) 7010.
[21] A. Heyden, A.T. Bell, F.K. Keil, J. Chem. Phys. 123 (2005) 224101.
[22] S. Nosé, J. Chem. Phys. 81 (1984) 511.
[23] W.G. Hoover, Phys. Rev. A 31 (1985) 1695.
[24] E.A. Carter, G. Ciccotti, J.T. Hynes, R. Kapral, Chem. Phys. Lett. 156 (1989) 472.
[25] W. K den Otter, W.J. Briels, Mol. Phys. 98 (2000) 773.
[26] E. Darve, M.A. Wilson, A. Pohorille, Mol. Simul. 28 (2002) 113.
[27] P. Fleurat-Lessard, T. Ziegler, J. Chem. Phys. 123 (2005) 084101.
[28] F. Eder, J.A. Lercher, Zeolites 18 (1997) 75.
[29] F. Eder, J.A. Lercher, J. Phys. Chem. B 101 (1997) 1273.
[30] F. Eder, M. Stockenhuber, J.A. Lercher, J. Phys. Chem. B 101 (1997) 5414.
[31] I.C. Gerber, J.G. Ángyán, J. Chem. Phys. 126 (2007) 044103.
[32] L. Benco, Th. Demuth, J. Hafner, F. Hutschka, H. Toulhoat, J. Chem. Phys. B 114 (2001) 6327.
[33] P.M. Esteves, M.A.C. Nascimento, C.J.A. Mota, J. Phys. Chem. B 103 (1999) 10417.
[34] J.A. Ryder, A.K. Chakraborty, A.T. Bell, J. Phys. Chem. B 104 (2000) 6998.
[35] X. Zheng, P. Blowers, J. Mol. Catal. A 229 (2005) 77.
[36] X. Zheng, P. Blowers, J. Phys. Chem. A 109 (2005) 1346.
[37] X. Zheng, P. Blowers, J. Mol. Catal. A 242 (2005) 18.
[38] X. Zheng, P. Blowers, J. Phys. Chem. A 110 (2006) 2455.
[39] R.A. van Santen, G.J. Kramer, Chem. Rev. 95 (1995) 637.
[40] F. Jensen, Introduction to Computational Chemistry, Wiley, Chichester, 1999, p. 301.
[41] A. Banerjee, N. Adams, J. Simons, R. Shepard, J. Chem. Phys. 89 (1985) 52.
[42] M.J.D. Powell, in: J.B. Rosen, O.L. Mangasarian, K. Ritter (Eds.), Nonlinear Programing, Academic Press, New York, 1970.

[43] M.J.D. Powell, Math. Prog. 1 (1971) 26.
[44] B. Murtagh, R.W.H. Sargent, Comput. J. 13 (1972) 185.
[45] J.M. Bofill, J. Comput. Chem. 15 (1994) 1.
[46] K. Fukui, Phys. Chem. 74 (1970) 4161.
[47] K. Fukui, Acc. Chem. Res. 14 (1981) 363.
[48] M.J. Janik, R.J. Davis, M. Neurock, J. Catal. 244 (2006) 65.
[49] J.P. Ryckaert, G. Ciccotti, H.J.C. Berendsen, J. Comput. Phys. 23 (1977) 327.